


## Analyzing quantum synchronization through Bohmian trajectories

Wenlin Li <sup>\*</sup>*Physics Division, School of Science and Technology, University of Camerino, I-62032 Camerino (MC), Italy*

(Received 2 June 2022; accepted 3 August 2022; published 15 August 2022)

We analyze quantum effects involved in continuous variable synchronization between two self-sustaining resonators in the framework of Bohmian mechanics. Bohmian trajectories provide visual descriptions of significant nonclassical dynamics, which allow us to characterize the level of quantum synchronization more intuitively compared with only utilizing some designed synchronization measures. It is found that in the quantum limit, the Bohmian trajectories will deviate from their corresponding semiclassical limit cycle behavior after they are distorted by the quantum potential. We explore the roles of zero-point fluctuation, superposition, and nonlocal correlation in synchronization dynamics, corresponding to the oscillators in a coherent state, superposition state, and entanglement state, respectively. We also explore the influence of squeezed Hamiltonian on spontaneous synchronization.

DOI: [10.1103/PhysRevA.106.023512](https://doi.org/10.1103/PhysRevA.106.023512)

### I. INTRODUCTION

The driven or spontaneous synchronization behavior [1,2] in microcosmic regime, namely quantum synchronization phenomenon, has recently attracted much attention in the field of quantum optics and quantum control. In the last decade, people have predicted and explored the possibility of synchronizing various quantum models, including spin subatomic particles and ensemble [3–10], Bose-Einstein condensation [11], quantum mechanical resonators [12–34], and cavity and circuit quantum electrodynamics system [4,7,35,36]. Among them, some representative schemes have been verified by experimental observations, most of which focus on continuous variable synchronization in cavity optomechanical systems (OMS) [37–39]. Concepts related to quantum synchronization are also active in the research of fundamental quantum theory, for example, cooperative synchronization is considered to be related to other quantum correlations [4,14–16,18,20], and provides explanations for the deep mechanisms of some quantum phenomena, such as phase transition [40,41] and spontaneous breaking of time translational symmetry in quantum many-body physics [19,42]. In the area of quantum information processing, quantum synchronization also shows its potential for the preparation of quantum entanglement resources [9] and the establishment of quantum networks [25].

Diverse microcosmic synchronization phenomena have inspired people to phenomenologically propose quantum synchronization definitions and measures from different perspectives, while these different versions are not compatible with each other [3,4,16,18,28,34,43]. Unlike concepts that are unique to quantum mechanics (e.g., entanglement), a convincing definition or description of quantum synchronization needs to respect the classical synchronization theory and be consistent with it in the classical limit. Previous research

has attempted to use mean-field theory to analyze quantum-classical synchronization crossover, where the expectation value with respect to the observable operator of the quantum system is considered as the classical dynamics, and the quantum properties are reflected by the fluctuations around the classical orbit [12–14,18,21,23,25,32]. Intuitively, this understanding presupposes that the quantum state corresponds to a single-peaked symmetric wave function in coordinate space such that the expectation value always has approximately the maximum probability of occurrence, so that its trajectories can be considered as the principal part of the dynamics. Conversely, this interpretation is no longer valid when the quantum state is of non-Gaussian or nonclassical properties [17,36,44,45]. Another idea for connecting classical and quantum synchronization is treating the results of quantum measurement with respect to quantum state as classical variables, which can be characterized by classical synchronization theory [18,46]. The controversial aspect of this treatment is that one has to face measurement-induced decoherence or collapse, and it levels regret that the synchronization theory relies on the measurement basis rather than on a purely dynamical analysis. This defect will become critical in the analysis of discrete variables synchronization as one has to consider various forms of positive operator-valued measurement (POVM) [47–50] instead of only homodyne or heterodyne measurement in continuous variable cases [51–53].

Moreover, a rigorous synchronization analysis requires examining the dynamic process of the system instead of only discussing certain states, even though the selected states are represented, such as the corresponding steady states [54]. In the classical regime, dynamical processes of a system are generally analyzed by deriving its effective potential [12,13,20,31,55], or by considering some non-Markovian factors, i.e., the synchronization measure of a certain moment  $t$  does not depend entirely on the state corresponding to that moment but requires the consideration of a segment of continuous trajectory in the time domain, such as the Pear-

<sup>\*</sup>wenlin.li@unicam.it

son's correlation coefficient [14–16,31,33,46]. Therefore, it is urgent to define a  $c$ -number potential and trajectory of a quantum system if one expects that the synchronization theory can be extended to the quantum regime.

For these purposes, we attempt to look for new perspectives on quantum synchronization and among them, synchronization analysis based on Bohmian mechanics may emerge as a potential alternative. Differing from the standard Copenhagen interpretation, Bohm proposed a quantum theory in 1952 that interprets a quantum system as an ensemble that is influenced by a quantum potential excited by its wave function, which is renamed a guided wave [56,57]. Here, we will not comment on the contribution of Bohm's interpretation to the fundamental concepts of quantum mechanics, however, it is undeniable that it offers a broad viewpoint on microscopic or mesoscopic properties and allows for intuitive visualization of quantum phenomena in terms of Bohmian trajectories [58–61]. For example, in the perspective of Bohm's interpretation, the quantum tunneling mechanism can be intuitively understood as the quantum potential filling the classical potential well, leading to a fraction of particles with higher initial energy being sufficient to cross the classical obstacle [62]. Subsequent research characterized further nonclassical phenomena, such as entanglement [63,64] and uncertainty principle [65,66], in the framework of Bohmian mechanics. In Bohm's interpretation, a quantum system is allowed to have explicit trajectories and  $c$ -number potential energy (although one degree of freedom is treated as a hidden variable), as well as an explicit classical counterpart model by neglecting the quantum potential, so it fits the challenges for analyzing quantum synchronization mentioned above.

In this paper, we investigate quantum complete synchronization and phase synchronization in the Bohmian picture by considering mechanical resonators in optomechanical systems as a platform. By introducing classical reservoir-system interaction into a quantum Hamilton-Jacobi equation, we generalize the Newton-like equations with respect to the Bohmian trajectories to a series of Bohmian-Langevin equations that can describe gain-dissipation balance mechanism in a quantum self-sustaining system [17,55]. These Bohmian trajectories correspond to wave function as the solution of a stochastic Schrödinger equation [52], which is sufficient to give a complete representation of quantum synchronization to compared that obtained by a Lindblad master equation [33]. We obtain the classical synchronization phase diagram of this model as a reference, subsequently, under the same classical parameter conditions, we examine the influence of significant nonclassical quantum effects, represented by zero-point fluctuation, superposition, and nonlocal correlations, on the synchronization, respectively, by analyzing the corresponding Bohmian trajectories. In addition, we also explore the influence of the squeezing Hamiltonian [28] on quantum synchronization.

The paper is organized as follows: In Sec. II, we investigate the self-sustaining oscillation behavior with respect to the oscillators of OMS in the Bohmian picture. In Sec. III, we analyze the synchronization phase diagram under the classical limit. Analysis of quantum synchronization based on Bohmian trajectories is given in Sec. IV and we finally summarize the results in Sec. V.

## II. SYSTEM OPEN DYNAMICS AND BOHMIAN QUANTUM TRAJECTORIES OF MULTIMODE OMS

The model we considered consists of two mechanical resonators optomechanically coupled to a high finesse Fabry-Pérot cavity driven by a pump laser beam, which will induce self-sustained limit cycles under appropriate parameters [13,31,55,67]. The two oscillators are also mutually interacting with each other via a phonon-exchange interaction with intensity  $\mu$  [18,68–70]. Experimentally, the considered model can also be implemented by a standard OMS coupled with another free mechanical resonator by phonon interaction after a parameter transformation [31,68]. In a rotating frame defined by  $\exp(-i\omega_c a^\dagger a)$ , the system Hamiltonian in the second quantization representation reads:

$$H/\hbar = \Delta \hat{a}^\dagger \hat{a} + iE(\hat{a}^\dagger - \hat{a}) - \mu(\hat{b}_1^\dagger \hat{b}_2 + \hat{b}_2^\dagger \hat{b}_1) + \sum_{j=1,2} \omega_{mj} \hat{b}_j^\dagger \hat{b}_j - g_j \hat{a}^\dagger \hat{a}(\hat{b}_j^\dagger + \hat{b}_j). \quad (1)$$

In this expression,  $\hat{a}$  ( $\hat{b}_j$ ) is the annihilation operator of the optical (the  $j$ th mechanical) field and  $\omega_c$  ( $\omega_m$ ) is the corresponding eigenfrequency.  $g_j$  is the single-photon coupling coefficient of the radiation pressure interaction. The pump laser is of intensity  $E$  and frequency  $\omega_d$  and  $\Delta = \omega_c - \omega_d$  is the detuning between the frequency of cavity and driving. By using the transformation

$$\hat{a} = \sqrt{\frac{m_c \Delta}{2\hbar}} \hat{x}_c + i \sqrt{\frac{1}{2\hbar m_c \Delta}} \hat{p}_c, \\ \hat{b}_j = \sqrt{\frac{m_j \omega_j}{2\hbar}} \hat{x}_j + i \sqrt{\frac{1}{2\hbar m_j \omega_j}} \hat{p}_j, \quad (2)$$

the Hamiltonian (1) can be rewritten in dimensional coordinate representation:

$$H = \left(1 - \sum_{j=1,2} \frac{g_j}{\Delta A_j} \hat{x}_j\right) \left(\frac{\hat{p}_c^2}{2m_j} + \frac{1}{2} m_c \Delta^2 \hat{x}_c^2\right) + \frac{2EA_c}{\hbar} \hat{p}_c - \frac{\mu}{2} \left(\frac{\hat{x}_1 \hat{x}_2}{A_1 A_2} + \frac{A_1 A_2}{\hbar^2} \hat{p}_1 \hat{p}_2\right) + \sum_{j=1,2} \frac{\hat{p}_j^2}{2m_j} + \frac{1}{2} m_j \omega_j^2 \hat{x}_j^2, \quad (3)$$

where  $m_j$  and  $A_j = \sqrt{\hbar/2m_j \omega_j}$  are the effective mass and the zero-point fluctuation amplitudes for the oscillators. Analogous to the case of oscillators, we define the effective mass of the cavity field as  $m_c = \hbar/2\Delta A_c^2$ , where  $A_c$  is the corresponding zero-point fluctuation amplitudes. Note that the cavity field will have a negative effective mass corresponding to the blue detuning ( $\Delta < 0$ ) case [71,72].

The one-dimensional Schrödinger equation in coordinate representation is defined by expressing momentum operators as  $\hat{p}_j = -i\hbar \nabla_j = -i\hbar \partial_{x_j}$  and  $\hat{p}_c = -i\hbar \nabla_c = -i\hbar \partial_{x_c}$ , which

reads:

$$i\hbar \frac{\partial \psi}{\partial t} = \left[ \left( 1 - \sum_{j=1,2} \frac{g_j}{\Delta A_j} x_j \right) \left( -\frac{\hbar^2}{2m_j} \nabla_c^2 \right) - i2EA_c \nabla_c + \frac{\mu A_1 A_2}{2} \nabla_1 \nabla_2 + \sum_{j=1,2} \left( -\frac{\hbar^2}{2m_j} \nabla_c^2 \right) + V(x_c, x_j) \right] \psi, \quad (4)$$

where  $V(x_c, x_j)$  is the corresponding classical potential:

$$V(x_c, x_j) = \left( 1 - \sum_{j=1,2} \frac{g_j}{\Delta A_j} x_j \right) \left( \frac{1}{2} m_c \Delta^2 x_c^2 \right) - \frac{\mu}{2} \frac{x_1 x_2}{A_1 A_2} + \sum_{j=1,2} \frac{1}{2} m_j \omega_j^2 x_j^2. \quad (5)$$

Now the wave function  $\psi$  is a complex function of dimensional coordinates  $(x_c, x_j)$  and time  $t$ , which can be reexpressed as:

$$\psi(x_c, x_j, t) = R(x_c, x_j, t) \exp \left[ i \frac{S(x_c, x_j, t)}{\hbar} \right], \quad (6)$$

by introducing two real variables  $R$  and  $S$ . Substituting Eq. (7) into the Schrödinger equation (5) and following the standard procedure for deriving Bohm potential [56], we can obtain the quantum Hamilton-Jacobi equation as:

$$\frac{\partial S}{\partial t} + T(x_c, x_j, t) + V(x_c, x_j, t) + U(x_c, x_j, t) = 0. \quad (7)$$

$T$  and  $V$  now can be regarded as kinetic energy and potential corresponding to a classical ensemble, and they together constitute a classical Hamiltonian:

$$\begin{aligned} H_c &= T(x_c, x_j, t) + V(x_c, x_j, t) \\ &= \left( 1 - \sum_{j=1,2} \frac{g_j}{\Delta A_j} x_j \right) \frac{(\nabla_c S)^2}{2m_c} \\ &\quad + \frac{2EA_c}{\hbar} \nabla_c S - \frac{\mu}{2} \frac{A_1 A_2}{\hbar^2} \nabla_1 S \nabla_2 S \\ &\quad + \sum_{j=1,2} \frac{(\nabla_j S)^2}{2m_j} + V(x_c, x_j, t), \end{aligned} \quad (8)$$

and  $U(x_c, x_j, t)$  is the quantum potential in Bohm's interpretation, which is expressed as:

$$\begin{aligned} U &= - \left( 1 - \sum_{j=1,2} \frac{g_j}{\Delta A_j} x_j \right) \frac{\hbar^2}{2m_c} \frac{\nabla_c^2 R}{R} \\ &\quad + \frac{\mu A_1 A_2}{2} \frac{\nabla_1 \nabla_2 R}{R} - \sum_{j=1,2} \frac{\hbar^2}{2m_j} \frac{\nabla_j^2 R}{R}. \end{aligned} \quad (9)$$

We emphasize here that, because the Hamilton-Jacobi equation we have obtained is equivalent to Schrödinger equation, all system's quantum properties have already been contained in the above quantum potential  $U$ , which will vanish in the classical limit ( $\hbar \rightarrow 0$ ).

By defining the conjugate quantities as  $(x_c, \nabla_c S)$  and  $(x_j, \nabla_j S)$ , the Hamilton-Jacobi equation can be transformed into a series of Newton-like equations including quantum forces  $-\nabla_c U$  and  $-\nabla_j U$  acting on the system, which can be written as:

$$\begin{aligned} d_t x_c &= \left( 1 - \sum_{j=1,2} \frac{g_j}{\Delta A_j} x_j \right) \frac{\nabla_c S}{m_c} + \frac{2EA_c}{\hbar}, \\ d_t \nabla_c S &= - \left( 1 - \sum_{j=1,2} \frac{g_j}{\Delta A_j} x_j \right) m_c \Delta^2 x_c - \nabla_c U, \\ d_t x_j &= \frac{\nabla_j S}{m_j} - \frac{\mu}{2} \frac{A_1 A_2}{\hbar^2} \nabla_{3-j} S, \\ d_t \nabla_j S &= -m_j \omega_j^2 x_j + \frac{\mu}{2} \frac{x_{3-j}}{A_1 A_2} - \nabla_j U \\ &\quad + \left( \frac{g_j}{\Delta A_j} \right) \left( \frac{(\nabla_c S)^2}{2m_c} + \frac{1}{2} m_c \Delta^2 x_c^2 \right). \end{aligned} \quad (10)$$

In Bohm's theory, the interpretation of generalized momentum  $\nabla_c S$  and  $\nabla_j S$  of each trajectory are regarded as hidden variables but not observations of momentum measurements of a quantum state, so that their corresponding accuracy is not constrained by the uncertainty principle. They will be consistent with momentum measurements corresponding to the standard quantum mechanical description, such as the momentum errors considered in previous CV quantum complete synchronization, by introducing a von Neumann measurement process [56].

Through the similar transformation to those in Eq. (2):  $\alpha = \sqrt{m_c \Delta / 2 \hbar} x_c + i \sqrt{1/2 \hbar m_c \Delta} \nabla_c S = (q_c + ip_c) / \sqrt{2}$  and  $\beta = \sqrt{m_j \omega_j / 2 \hbar} x_j + i \sqrt{1/2 \hbar m_j \omega_j} \nabla_j S = (q_j + ip_j) / \sqrt{2}$ , we rewrite Eq. (11) into dimensionless equations for convenient:

$$\begin{aligned} \dot{\alpha} &= -i \left[ \Delta - \sum_j g_j (\beta_j + \beta_j^*) \right] \alpha + E - i \tilde{\nabla}_c \tilde{U}, \\ \dot{\beta}_j &= -i \omega_{mj} \beta_j + i \sum_j g_j |\alpha|^2 + i \mu \beta_{3-j} - i \tilde{\nabla}_j \tilde{U}, \end{aligned} \quad (11)$$

with the dimensionless quantum potential:

$$\begin{aligned} \tilde{U} &= - \left( \Delta - \sum_{j=1,2} g_j (\beta_j + \beta_j^*) \right) \frac{\tilde{\nabla}_c^2 R}{R} \\ &\quad + \frac{\mu}{2} \frac{\tilde{\nabla}_1 \tilde{\nabla}_2 R}{R} - \sum_{j=1,2} \omega_j \frac{\tilde{\nabla}_j^2 R}{R}, \end{aligned} \quad (12)$$

where the modified Laplace operators  $\tilde{\nabla}_j = \partial_{q_j}$  and  $\tilde{\nabla}_c = \partial_{q_c}$ .

An isolated OMS can be completely characterized by Bohmian trajectories obtained by Eq. (11) with correct initial conditions. However, the dissipation effect, including the decay of the cavity and the influence of the Brownian motion acting on the oscillators, can not be ignored if we focus on the phenomenon dominated by the nonlinear effect. Dissipation can also be analyzed in Bohmian representation by considering all the freedom of reservoir and reservoir-system interaction and the previous research related to open quantum system theory show the corresponding Hamiltonian are  $H_r = \sum_k (\omega_k \hat{a}_k^\dagger \hat{a}_k + \sum_{j=1,2} \omega_k \hat{b}_{j,k}^\dagger \hat{b}_{j,k})$

and  $H_{rs} = v_c(\omega_k)\hat{a}_k^\dagger\hat{a} + \sum_{j=1,2} v_j(\omega_k)\hat{b}_k^\dagger\hat{b}_j + \text{H.c.}$ , respectively [25,73,74]. Here we assume the reservoir is expected to behave almost classically, in particular, the quantum potential and force induced by  $H_r$  and  $H_{rs}$  are negligible [57]. Under this hypothesis, reservoir and reservoir-system interaction will be described by classical Hamiltonian obtained by replacing the operators in  $H_r$  and  $H_{rs}$  with  $c$  numbers. After solving the degrees of freedom of the reservoir and substituting the solutions into Eq. (11), we can obtain a set of differential-integral equations as:

$$\begin{aligned} \dot{\alpha} &= -i \left[ \Delta - \sum_j g_j(\beta_j + \beta_j^*) \right] \alpha + E - i\tilde{\nabla}_c\tilde{U}, \\ &\quad - \sum_k v_c(\omega_k) e^{-i(\omega_k - \omega_c)(t-t_0)} a_k(t_0) \\ &\quad - \sum_k \int_{t_0}^t dt' e^{-i(\omega_k - \omega_c)(t-t')} \alpha(t'), \\ \dot{\beta}_j &= -i\omega_{mj}\beta_j + i \sum_j g_j|\alpha|^2 + i\mu\beta_{3-j} - i\tilde{\nabla}_j\tilde{U} \\ &\quad - \sum_k v_j(\omega_{j,k}) e^{-i(\omega_k - \omega_{m,j})(t-t_0)} b_{j,k}(t_0) \\ &\quad - \sum_k \int_{t_0}^t dt' e^{-i(\omega_k - \omega_{m,j})(t-t')} \beta(t'). \end{aligned} \quad (13)$$

By assuming that the coupling intensity of reservoir-system interaction is a flat spectrum without frequency dependence, the above differential-integral equations will degenerate back to the following Langevin equation without any memory effect:

$$\begin{aligned} \dot{\alpha} &= \left[ -\kappa - i \left( \Delta - \sum_j g_j(\beta_j + \beta_j^*) \right) \right] \alpha \\ &\quad + E - i\tilde{\nabla}_c\tilde{U} + \sqrt{2\kappa}\alpha_{\text{in}}, \\ \dot{\beta}_j &= (-\gamma_j - i\omega_{mj})\beta_j + i \sum_j g_j|\alpha|^2 \\ &\quad + i\mu\beta_{3-j} - i\tilde{\nabla}_j\tilde{U} + \sqrt{2\gamma_j}\beta_{j,\text{in}}, \end{aligned} \quad (14)$$

where  $\kappa$  and  $\gamma_j$  are amplitude decay rates of the cavity and mechanical oscillator, respectively.  $\alpha_{\text{in}}$  and  $\beta_{\text{in}}$  are the input reservoir noise. Under Markovian approximation, they are assumed to be white Gaussian noises obeying standard correlation function:  $\langle \alpha_{\text{in}}(t)^* \alpha_{\text{in}}(t') \rangle = \delta_{jj'}/2$  and  $\langle \beta_{\text{in}}(t)^* \beta_{\text{in}}(t') \rangle = (\bar{n}_b + 1/2)\delta_{jj'}$ , where  $\bar{n}_b = [\exp(\hbar\omega_j/k_bT) - 1]^{-1}$  is the mean occupation number of the mechanical bath and it gauges the temperature  $T$  of the system [75]. In the case of mechanical oscillators are of high-quality factors ( $\omega_{m,j}/\gamma_j \gg 1$ ), the dissipation terms  $-\kappa\alpha$  and  $-\gamma_j\beta_j$  can well correspond to a non-Hermitian Hamiltonian  $H_{\text{eff}}/\hbar = (\Delta - i\kappa)\hat{a}^\dagger\hat{a} + \sum_j(\omega_{m,j} - i\gamma_j)\hat{b}_j^\dagger\hat{b}_j$ . Moreover, we can also reconstruct a stochastic Hamiltonian according to the stochastic fluctuation noise terms, so that Langevin equations of Bohmian trajectories can well correspond to a stochastic Schrödinger

equation [52]:

$$i\hbar d_t |\tilde{\psi}\rangle = H_{\text{eff}} |\tilde{\psi}\rangle + i\hbar \sum_k \xi_k L_k |\tilde{\psi}\rangle, \quad (15)$$

where the five Lindblad operators are  $L_1 = \sqrt{2\kappa}\hat{a}$ ,  $L_2 = \sqrt{2\gamma_1}(\bar{n}_b + 1)\hat{b}_1$ ,  $L_3 = \sqrt{2\gamma_1}\bar{n}_b\hat{b}_1^\dagger$ ,  $L_4 = \sqrt{2\gamma_2}(\bar{n}_b + 1)\hat{b}_2$ , and  $L_5 = \sqrt{2\gamma_2}\bar{n}_b\hat{b}_2^\dagger$ , respectively, and  $\xi_k = dW_k/dt$  is a white noise and  $W_k$  corresponds to a Wiener stochastic increments. In this expression, wave vector  $|\tilde{\psi}\rangle$  is an unnormalized state vector since up to now we only consider the Hamilton-Jacobi equation part of Bohm's interpretation. Considering that the flow conservation equation will preserve the norm of quantum state and respecting the fact that the classical environment will not modify the flow equation under our assumption, we finally map the Langevin equations to the normalized form of Eq. (15) [33,52]:

$$\begin{aligned} id_t |\psi\rangle &= \left[ \frac{H_{\text{eff}}}{\hbar} + i \sum_k \frac{\langle L_k + L_k^\dagger \rangle}{2} \left( L_k - \frac{\langle L_k + L_k^\dagger \rangle}{4} \right) \right] |\psi\rangle \\ &\quad + i \sum_k \xi_k \left( L_k - \frac{\langle L_k + L_k^\dagger \rangle}{2} \right) |\psi\rangle, \end{aligned} \quad (16)$$

and the above stochastic Schrödinger equation will reduce to following standard Lindblad master equation:

$$\begin{aligned} \dot{\rho} &= -i[H/\hbar, \rho] + \kappa \mathcal{L}[\hat{a}]\rho \\ &\quad + \sum_{j=1,2} \gamma_j(\bar{n}_b + 1)\mathcal{L}[\hat{b}_j]\rho + \gamma_j(\bar{n}_b)\mathcal{L}[\hat{b}_j^\dagger]\rho, \end{aligned} \quad (17)$$

by taking the average over stochastic wave vector  $|\psi\rangle$ . Here  $\mathcal{L}[\hat{\rho}]\rho = 2\hat{\rho}\rho\hat{\rho}^\dagger - \hat{\rho}^\dagger\hat{\rho}\rho - \rho\hat{\rho}^\dagger\hat{\rho}$  is the standard form of the Lindblad superoperator. Equations (15) and (16) can help us simplify the calculation or save computational resources. In particular, when the corresponding energy of the whole system is in the order of several quanta ( $\langle \hat{a}^\dagger\hat{a} \rangle \sim \langle \hat{b}_j^\dagger\hat{b}_j \rangle \sim [10^0, 10^1]$ ), we can use a truncated Hilbert space to simulate the stochastic Schrödinger equation instead of adopting the drift-diffusion equation, and a convenient way of obtaining Bohmian trajectories is to solving Eqs. (15) or (16) for the wave function in Fock basis, and then to use the relations,

$$|m\rangle \rightarrow \psi_m(q) = \frac{1}{\sqrt{2^m m! \sqrt{\pi}}} H_m(q) e^{(-q^2/2)}, \quad (18)$$

and

$$\begin{aligned} R^2 &= \text{Re}(\psi)^2 + \text{Im}(\psi)^2, \\ S &= \tan^{-1}[\text{Im}(\psi)/\text{Re}(\psi)], \end{aligned} \quad (19)$$

and substituting  $\tilde{\nabla}_c S$  and  $\tilde{\nabla}_{q_j} S$  into Eq. (14) [56].

Now let us reexamine the above derivations; the only approximation we adopted is regarding the reservoir as classical ensembles, which results in that there is no related correction term induced by the dissipation in the expression of the quantum potential. In contrast, other quantum effects are completely contained in Langevin equations of Bohmian trajectories, including quantum interference or quantum entanglement among subsystems.

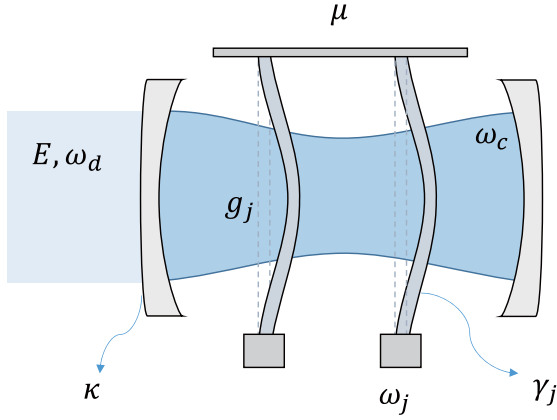


FIG. 1. Schematic diagram of an OMS consists of two membranes. Here one mechanical resonator coupled with the other resonator by a beam-splitter interaction.

### III. SYNCHRONIZATION CORRESPONDING TO CLASSICAL LIMIT

Before analyzing synchronization in the quantum regime, as a comparison, here we briefly introduce some corresponding synchronization properties under the classical limit. In the case the quantum potential can be ignored, the multimode OMS we consider can be mapped to a classical ensemble, in which each element will satisfy a set of stochastic Langevin equations. In fact, those stochastic equations have provided a semiclassical perspective for the analysis of quantum synchronization in previous work [17,22,31,46]. Once classical synchronization occurs, the noise terms have only negligible disturbance to the synchronization effect in this model: they only promote the diffusion of the total phase, by contrast, the behavior of amplitude and phase difference are bound around their corresponding mean value due to the dissipation and correlation [31]. This implies that noiseless dynamic equations are sufficient to give the relevant information of synchronization, which can be written as:

$$\begin{aligned} \dot{\alpha} &= \left[ -\kappa - i \left( \Delta - \sum_j g_j (\beta_j + \beta_j^*) \right) \right] \alpha + E, \\ \dot{\beta}_j &= (-\gamma_j - i\omega_{mj})\beta_j + i \sum_j g_j |\alpha|^2 + \mu\beta_{3-j}, \end{aligned} \quad (20)$$

where  $\alpha$  and  $\beta_j$  can also be regarded as mean values corresponding to the optical field and oscillators of the classical ensemble. Under the condition  $Eg_j/\omega_{mj} \ll 1$ , the general solution of Eq. (20) can be described by the ansatz  $\beta_j(t) = B_j + I_j e^{i\theta_j}$  [13,55], and one can approximately regard  $I_j \rightarrow 0$  or  $B_j \rightarrow 0$  depending on whether each mechanical resonator corresponding to an asymptotic stable or self-sustained limit cycle dynamics. As it has been analyzed in Refs. [13,24,31] that obvious phase synchronization can occur in this model because the stable oscillator amplitudes ( $I_j \sim 0$ ) in the long-time regime leading to the evolution of phase difference  $\theta_- = \theta_1 - \theta_2$  to satisfy a Kuramoto-type equation, in which the coupling coefficient is related to the ratio of two oscillator amplitudes, which is sensitive to the intensity of the radiation pressure  $g$  and phonon-exchange interaction  $\mu$ . In

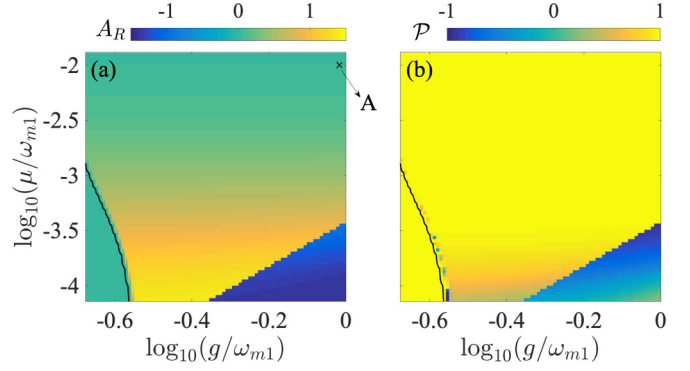


FIG. 2. (a), (b) Amplitude ratio [ $A_R = \log_{10}(|\beta_1|/|\beta_2|)$ ] and synchronization phase diagrams in terms of  $\mathcal{P}$  in the  $g$ - $\mu$  plane. The black (dark) dashed line in each subfigure denote the boundary between asymptotic steady-state phase and limit cycle phase. The other characteristic parameters of the OMS are  $\omega_{m1} = 2\pi \times 235$  kHz and  $\omega_{m2} = 2\pi \times 235.5$  kHz,  $\kappa = 2\pi \times 170$  kHz,  $\gamma_1 = \gamma_2 = 20$  Hz, and  $E/\omega_{m1} = 0.0184$ .

Fig. 2(a), we first show the amplitude ratio of the two oscillators in the  $g$ - $\mu$  plane obtained from a long time numerical solution of Eq. (20), and the corresponding synchronization phase diagram, characterizing by a simple measure  $\mathcal{P} = \int_0^T \cos[\theta_1(t) - \theta_2(t)] dt / T$ , is plotted in Fig. 2(b). They show that the contours of the two subfigures are well consistent with each other. In the case of the phonon-exchange interaction is weak, mode competition between two mechanical modes occurs [76], and the corresponding amplitude ratio will first reach  $|\beta_1|/|\beta_2| \sim 20$  and directly reverse to  $|\beta_1|/|\beta_2| \sim 0.04$ , accompanied by an in-phase or antiphase synchronization transition. With the increase of  $\mu$ , the gradually balanced energy will inhibit the mode competition, so that the two oscillators have close amplitudes while the phase is perfectly locked, that is, they have achieved complete synchronization.

### IV. QUANTUM SYNCHRONIZATION ANALYSIS BASED ON BOHMIAN QUANTUM TRAJECTORIES

Now we explore the influence of quantum effects, mainly coherence and nonlocality, on synchronization beyond classical dynamics by investigating the evolution of different initial states under Hamiltonian (1). In the following discussion, we will focus on the case of  $\mu/\omega_{m1} = 0.01$  and  $g/\omega_{m1} = 0.9629$ , corresponding to the point A in the phase diagram Fig. 2 so that we can study the case of phase synchronization and complete synchronization simultaneously. In order to eliminate the influence of classical dynamics on the system, the initial states are prepared according to the following process: we first select a class of quantum states whose mean values correspond to the field operators  $\hat{a}$  and  $\hat{b}_j$  close to zero, and then through a translation operation, we ensure that these states center at the classical orbit corresponding to equation (20), that is:

$$|\psi_{t_0}\rangle = D(\alpha)D(\beta_1)D(\beta_2)|\phi\rangle, \quad (21)$$

where  $D(\alpha) = \exp(\alpha\hat{a}^\dagger - \alpha^*\hat{a})$  and  $D(\beta_j) = \exp(\beta_j\hat{b}_j^\dagger - \beta_j^*\hat{b}_j)$  are standard operation operators and we require that

$\langle \phi | \hat{b}_j | \phi \rangle \ll |\beta_j|$ . So the quantum properties of  $|\psi_{t_0}\rangle$  will depend on the form of  $|\phi\rangle$  we selected.

The complete synchronization in the framework of Bohmian mechanics is investigated by the coordinate errors  $q_1^j - q_2^j$ , where the superscript  $j$  denotes the  $j$ th Bohmian trajectory of each oscillator. Considering that the quantum potential may distort the single-mode oscillation behavior of some trajectories, the phase synchronization is further determined by the Pearson's correlation coefficient:

$$C_{q_1^j, q_2^j}(t, \Delta t) = \frac{\overline{\delta q_1^j \delta q_2^j}}{\sqrt{\overline{\delta(q_1^j)^2} \times \overline{\delta(q_2^j)^2}}}, \quad (22)$$

where  $\bar{o} = \Delta t^{-1} \int_t^{t+\Delta t} o(\tau) d\tau$  and  $\delta o = \bar{o} - o$ . Based on the Pearson's coefficient, we define logarithmic Pearson's correlation coefficient  $C'$  as:

$$C'_{q_1^j, q_2^j}(t, \Delta t) = \log_2 [1 - C_{q_1^j, q_2^j}(t, \Delta t)]. \quad (23)$$

The Pearson's coefficient yield  $C = 1, 0$ , and  $-1$  when the system is zero-phase synchronized, unsynchronized, and  $\pi$ -phase synchronized, so that the range of logarithmic Pearson's correlation coefficient  $C'$  is  $-\infty$  to  $1$ , corresponding to the system is zero-phase synchronized and  $\pi$ -phase synchronized, respectively.

#### A. Quantum synchronization behavior induced by zero-point fluctuation

We first discuss the effect of zero-point fluctuation on quantum synchronization by setting  $|\phi\rangle = |0\rangle_c |0\rangle_{m1} |0\rangle_{m2}$ , that is, both the oscillators and the cavity field correspond to vacuum states, in which case  $|\psi_{t_0}\rangle$  will become a coherent state  $|\phi\rangle = |\alpha\rangle_c |\beta_1\rangle_{m1} |\beta_2\rangle_{m2}$ . The complete characterization of a quantum system requires a series of Bohmian trajectories with different initial conditions. In the following discussion, for convenience, we only analyze those trajectories whose initial condition of cavity field is  $q_c = \sqrt{2} \langle \psi_{t_0} | \hat{c} | \psi_{t_0} \rangle$  and the initial positions of each oscillator are set as nine different values, which, respectively, are:  $q_j(0) - \sqrt{2} \langle \psi_{t_0} | \hat{b}_j | \psi_{t_0} \rangle = 0, \pm 0.1, \pm 0.2, \pm 0.3, \pm 0.4$ . We consider all possible combinations of these initial positions, that is, a total of 81 Bohmian trajectories are calculated to describe the quantum synchronization behavior of the resonators. The values of these initial positions are plotted in Fig. 3(a), where we classify identical initial positions corresponding to oscillator 1 into one set and mark them with the same color. In Fig. 3(b), we plot the probability amplitude  $R(q_c, q_1, q_2)$  of  $|\psi_{t_0}\rangle$  and the corresponding quantum potential  $\tilde{U}(q_c, q_1, q_2)$  in coordinate space. The contour lines show that a Gaussian wave packet with a single peak corresponds to a monotonic repulsive potential, which resists the amplitude noise suppression induced by nonlinear dynamics, resulting in the Bohmian trajectories with less bunching in phase space compared with semiclassical trajectories. Dynamics behaviors of Bohmian trajectories are shown in Figs. 3(c) and 3(d) corresponding to mechanical resonator 1 and 2, respectively. These oscillating trajectories can be regarded as a series of identical trajectories, which are translated to different positions by quantum potential energy according to the corresponding initial position. This

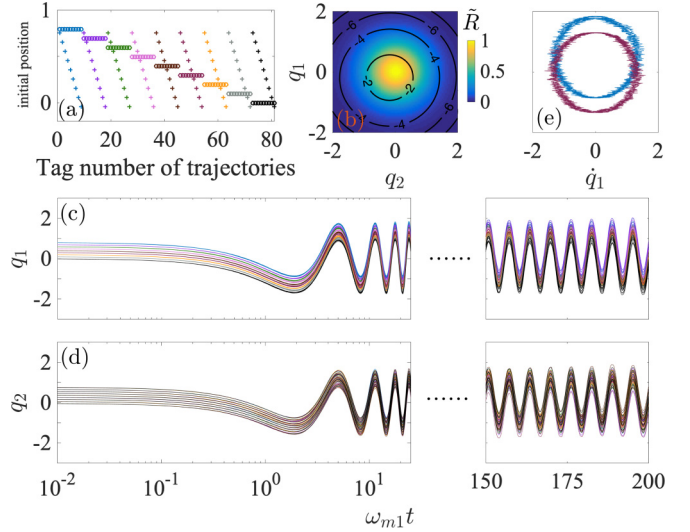


FIG. 3. (a) The initial positions corresponding to 81 Bohmian trajectories we calculated. The corresponding trajectory of each point is marked with the same color in the following subfigures. (b) The  $z$  axis represents the normalized probability amplitude  $\tilde{R} = R(q_c, q_1, q_2) / \max[R(q_c, q_1, q_2)]$  with respect to the wave function  $|\psi_{t_0}\rangle$  and the contour lines corresponding to the dimensionless quantum potential  $\tilde{U}(q_c, q_1, q_2)$ . Here we fix the value of  $q_c$  as  $q_c = \sqrt{2} \text{Re}(\langle c \rangle)$ . (c) and (d) The Bohmian trajectories corresponding to the resonators 1 and 2, respectively. (e) Orbit of Bohmian trajectory with respect of resonators 1 in the phase space  $\text{span}\{q_1, \dot{q}_1\}$ . Here the blue (lower) limit cycle corresponds to  $q_1(0) = \sqrt{2} \langle \psi_{t_0} | \hat{b}_1 | \psi_{t_0} \rangle$ ,  $q_2(0) = \sqrt{2} \langle \psi_{t_0} | \hat{b}_2 | \psi_{t_0} \rangle$  (trajectory No. 41), and the purple (upper) limit cycle corresponds to  $q_1(0) = \sqrt{2} \langle \psi_{t_0} | \hat{b}_1 | \psi_{t_0} \rangle + 0.5$ ,  $q_2(0) = \sqrt{2} \langle \psi_{t_0} | \hat{b}_2 | \psi_{t_0} \rangle$  (trajectory No. 1). Here the evolution wave function is numerically simulated in a  $(3 \times 3)_c \otimes (40 \times 40)_{m1} \otimes (40 \times 40)_{m2}$  Hilbert subspace with the Fock-state basis, and the other parameters are the same as those of Fig. 1.

conclusion can also be reflected by parallel limit cycles in the phase space  $\text{span}\{q_1, \dot{q}_1\}$ , as shown in Fig. 3(e). Moreover, the same colored trajectories in Fig. 3(c) almost coincide in the subsequent evolution, which means that one resonator has a weak effect on the evolution of the other one, that is, the correlation between the two resonators is still weak, although they are already synchronized in the classical regime.

Figure 4(a) illustrates that trajectories of coordinate differences are also almost parallel to each other. As a contrast, we also plot the expected value of the coordinate error obtained by simulating master equation Eq. (17) in this subfigure. It can be also seen that the Bohmian trajectories do not provide any more qualitative information except error fluctuation in this case. These phenomena reveal that the repulsive effect of the quantum potential only has negligible effect on quantum synchronization in the framework of Bohmian mechanics. Specifically, the zero-point fluctuation seems to be neither enhanced nor disturbed by quantum synchronization, which is different from the input Langevin noise induced by reservoir. This conclusion will be more obvious when investigating phase synchronization, as shown in Fig. 4(b), the Pearson's coefficients corresponding to different trajectories are clustered in a very small range. It is also worth noting that since the considered Bohmian trajectories are determined by the

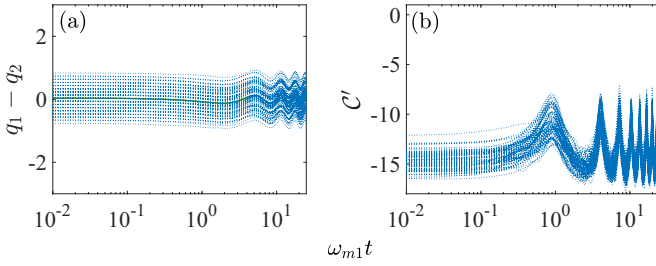


FIG. 4. (a) The dashed blue lines are the 81 trajectories of coordinate differences  $q_1^j - q_2^j$  obtained by Bohmian trajectories and the solid green line denotes the corresponding expected value obtained by simulating the master equation (17). (b) Logarithmic Pearson's correlation coefficients  $\mathcal{C}$  correspond to the Bohmian trajectories. Here the parameters are the same as those of Fig. 2.

stochastic Schrödinger equation (15), Fig. 4(a) actually reproduces the conclusion in Ref. [33], that is, the stochastic Schrödinger equation can provide consistent synchronization analysis with that given by Lindblad master equation, at least in the case of corresponding mixture of Gaussian state (limit cycle state).

### B. Synchronization between superposition or entangled states

In the case where  $|\phi\rangle$  is not a vacuum state, the considered state  $|\psi_{t_0}\rangle$  will be a non-Gaussian state, which corresponds to a Wigner function with a negative value and shows non-negligible quantum properties. Here we mainly focus on the relationship between entanglement and synchronization by setting  $|\phi\rangle$  as a typical Bell-type entangled state:

$$|\phi\rangle = |0\rangle_c \otimes (g|00\rangle + f e^{i\theta}|11\rangle)_{m_1, m_2}, \quad (24)$$

where  $|g|^2 + |f|^2 = 1$ . The translation operators  $D(\alpha)$  and  $D(\beta_j)$  corresponding to local unitary (LU) operations, so  $|\phi\rangle$  and  $|\psi_{t_0}\rangle$  are equivalent when only the properties of related to entanglement are considered. In Fig. 5, we plot Bohmian trajectories corresponding to the case of  $g = f$ , where  $|\phi\rangle$  has the maximum degree of entanglement. Compared with the dynamic behavior shown in Figs. 3(c) and 3(d), Figs. 5(a)–5(d) show that the two oscillators deviate from the semiclassical cosine-type oscillation under the influence of the quantum potential more obviously, and the shape of these trajectories become sensitive to the initial position so that they are no longer parallel to each other. Moreover, one oscillator significantly affects the dynamics behavior of the other oscillator in this case, which is reflected in Figs. 5(a) and 5(b) that the same-colored trajectories no longer coincide with each other soon. It is worth noting that in Sec. IV A, we explained that classical dynamics with zero-point fluctuation can cause only weak correlation in the considered time regime. Therefore, such apparent interaction between two oscillators can be regarded as induced by quantum correlation. The analysis of complete synchronization is shown in Figs. 5(e) and 5(f). Even if the synchronized quantum states have the maximum degree of entanglement, the dynamic behavior of their error is not significantly different from the semiclassical case if only the corresponding expected value is considered. The influence of quantum effect is manifested by errors of Bohmian

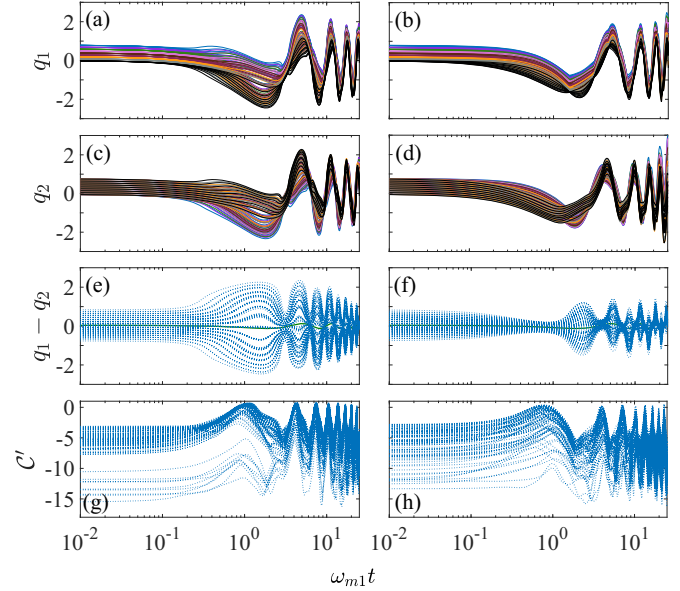


FIG. 5. Characterization of quantum synchronization with respect to entanglement state (24) by using Bohmian trajectories. The left column (a), (c), (e), (g) corresponds to the case of  $g = f = 1/\sqrt{2}$  and  $\theta = 0$  and the right column (b), (d), (f), (h) corresponds to the case of  $g = f = 1/\sqrt{2}$  and  $\theta = \pi/2$ . The Bohmian trajectories corresponding to the resonators 1 and 2 are shown in (a), (b) and (c), (d), respectively. In (e) and (f), the dashed blue lines are the trajectories of coordinate differences  $q_1^j - q_2^j$  obtained by Bohmian trajectories and the solid green line denotes the corresponding expected value obtained by simulating the master equation (17). (g) and (h): Logarithmic Pearson's correlation coefficients  $\mathcal{C}'$  correspond to the Bohmian trajectories. Here the parameters are the same as those of Fig. 2.

trajectories, which are alternating between two states of bunching and repelling others. Therefore, we can conclude that the influence of entanglement on the synchronization in the whole dynamics is not invariable but presents an effect of alternately enhancing and disturbing synchronization. The conclusion with respect to the phase synchronization is similar, and the Pearson's factor fluctuates in a larger range. In Figs. 6(a) and 6(c) we show that the probability amplitude and the corresponding quantum potential with respect to the entangled initial state  $|\psi_{t_0}\rangle$  have a more complex shape, which is the essence of entanglement inducing relevant dynamics. The case corresponding to  $\omega_{m1}t = 250$  is shown in Figs. 6(b) and 6(d), which shows that the quantum state will degenerate to a single-peak wave function without superposition under the influence of noise. At this time, the quantum effect will correspond to the negligible repulsive potential, similar to the case of coherent states.

We then consider the second entangled state, which is expressed as:

$$\begin{aligned} |\psi_{t_0}\rangle &= \mathcal{N}(|\psi_{t_0}^1\rangle + |\psi_{t_0}^2\rangle) \\ &= \mathcal{N}(|\alpha\rangle_c |\beta_1\rangle_{m_1} |\beta_2\rangle_{m_2} + e^{i\theta} |\alpha'\rangle_c |\beta'_1\rangle_{m_1} |\beta'_2\rangle_{m_2}), \end{aligned} \quad (25)$$

where  $\mathcal{N} = (2 + e^{-i\theta} \langle \alpha' \beta'_1 \beta'_2 | \alpha \beta_1 \beta_2 \rangle + \text{c.c.})^{-1/2}$  is the normalization constant. The physical meaning of the entangled state in this expression represents the coherent superposition

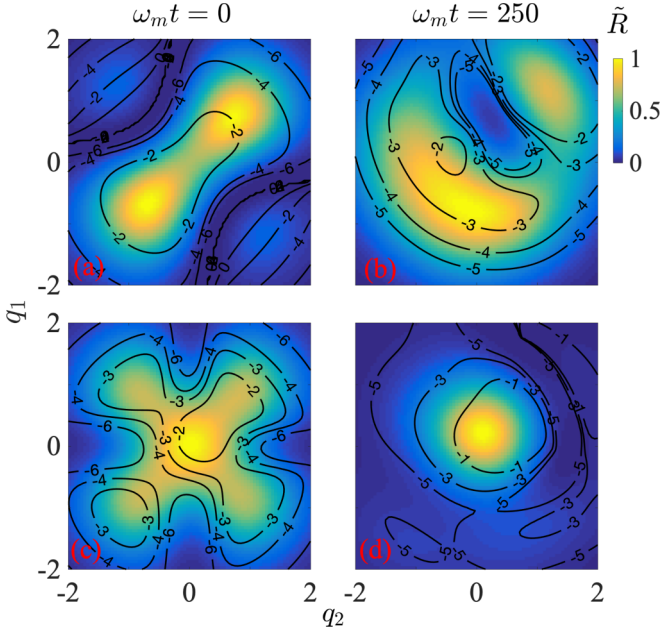


FIG. 6. The  $z$  axis represents the normalized probability amplitude  $\tilde{R} = R(q_c, q_1, q_2) / \max[R(q_c, q_1, q_2)]$  with respect to the wave function  $|\psi\rangle$  at  $\omega_m t = 0$  (a), (c) and  $\omega_m t = 250$  (b), (d), respectively. The contour lines corresponding to the dimensionless quantum potential  $\tilde{U}(q_c, q_1, q_2)$ . Here we set  $\theta = 0$  for (a) and (b) and  $\theta = \pi/2$  for (c) and (d). Here the parameters are the same as those of Fig. 5.

of two possible synchronization states, while in the above discussion, we translate the entangled quantum state to a point on the classical limit cycle, that is, a single synchronization state with entanglement. Intuitively, synchronization will not only reflect the respective properties of  $|\psi^1\rangle$  and  $|\psi^2\rangle$ , but also be affected by their interference. For each oscillator, we consider three sets of initial positions, which are

$$\begin{cases} \sqrt{2}\langle\psi_{t_0}^1|\hat{b}_j|\psi_{t_0}^1\rangle + \{0, \pm 0.05, \pm 0.1\}, & (26a) \\ \sqrt{2}\langle\psi_{t_0}^2|\hat{b}_j|\psi_{t_0}^2\rangle + \{0, \pm 0.05, \pm 0.1\}, & (26b) \\ \sqrt{2}\langle\psi_{t_0}|\hat{b}_j|\psi_{t_0}\rangle + \{0, \pm 0.05, \pm 0.1\}, & (26c) \end{cases}$$

and all possible combinations of each set are calculated, that is, we use a total of  $15 \times 15 = 225$  Bohmian trajectories to characterize the dynamics of the two oscillators. We use different colors to distinguish trajectories whose initial positions belong to different sets and plot their dynamic behavior in Fig. 7. Roughly speaking, the three sets of initial positions will induce the trajectories to have three kinds of phases. Nevertheless, the phase differences between the trajectories corresponding to oscillator 1 and oscillator 2 are still locked, as shown in Figs. 7(e) and 7(f). In Figs. 8(a) and 8(b), we select and plot some representative trajectories, which are mainly concentrated near the expected value  $q_j(0) = \sqrt{2}\langle\psi_{t_0}|\hat{b}_j|\psi_{t_0}\rangle$  and are more sensitive to the quantum interference effect. Bohmian trajectories corresponding to the solid lines with opposite phases represent, respectively, the independent properties of  $|\psi^1\rangle$  and  $|\psi^2\rangle$ , while the dotted lines show the alternating swing between these two phases caused by coherent superposition. In order to explain the phase swing

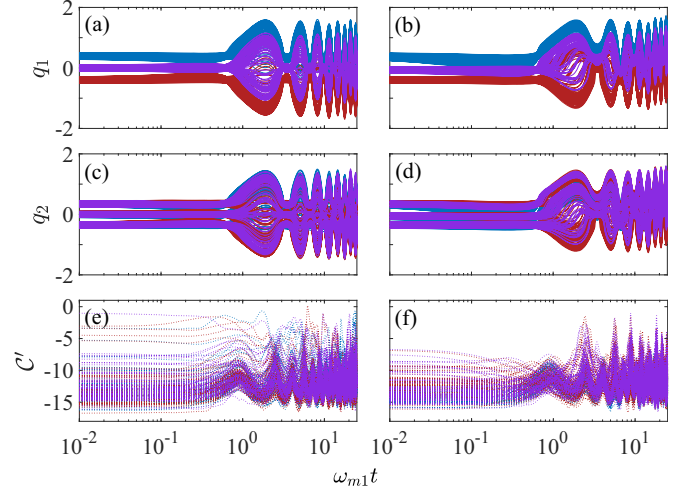


FIG. 7. Characterization of quantum synchronization with respect to entanglement state (25) by using Bohmian trajectories. The left column (a), (c), (e) corresponds to the case of  $\theta = 0$  and the right column (b), (d), (f) corresponds to the case of  $\theta = \pi/2$ . The blue [top in (a)], red [middle in (a)] and purple [bottom in (a)] lines denote those trajectories whose initial positions of oscillator 1 corresponds to Eqs. (26a), (26b), (26c), respectively. Here the parameters are the same as those of Fig. 2.

more intuitively, we select the upper trajectories in Figs. 8(a) and 8(b) as the benchmarks, we calculate the correlation coefficients between them and the other two trajectories, and show the result in Figs. 8(c) and 8(d). It is worth noting that one can also observe two kinds of phase evolution in an ensemble in the case of mixed synchronization composed of mixed superposition  $\rho \propto (|\psi^1\rangle\langle\psi^1| + |\psi^2\rangle\langle\psi^2|)$  [17,22,31], however, such kind of swinging between the two phases is a unique phenomenon caused by coherent superposition  $|\psi\rangle \propto (|\psi^1\rangle + |\psi^2\rangle)$ . The probability amplitude and the corresponding quantum potential of  $|\psi_{t_0}\rangle$  are plotted in Figs. 8(e) and 8(f). It can be seen that they correspond to a bimodal structure, while each peak corresponds to repulsive potential energy, and the part between the two peaks can induce a relevant dynamic effect. An intuitive inference is that if the peaks corresponding to a superposition state are far away in the coordinate space, their interference effect will be weak, while the Bohmian trajectories only represent the independent properties of each peak, which is similar to the case of mixed superposition.

### C. Impact of squeezing on synchronization

Another issue worth exploring in quantum synchronization is the effect of squeezing on synchronization. Reference [28] has investigated a single self-sustaining quantum oscillator driving by a squeezing Hamiltonian. The  $U(1)$  symmetry in this model is destroyed by even small values of squeezing while the oscillator has a nonclassical steady state, which deviates significantly from the limit cycle state [34]. For the concept of spontaneous mutual synchronization, recently, how it will be affected by some indirect squeezing effect, such as the oscillators coupled with a squeezed optical field in an OMS, is also discussed by Ref. [27].



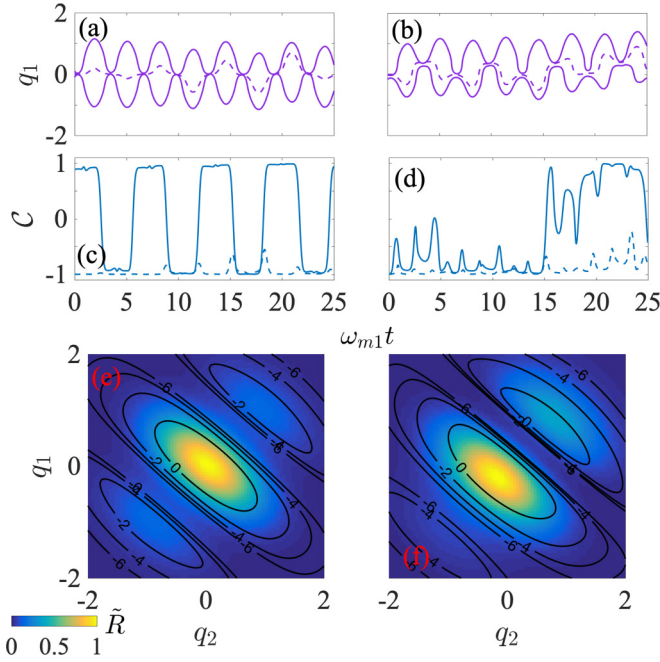


FIG. 8. (a) and (b) Representative trajectories selected from Figs. 7(a) and 7(b), respectively. (c) and (d) The solid lines denote Pearson's correlation coefficients between the top and the middle trajectories in (a) and (b) and the dash lines are the same factor between the top and the bottom trajectories. (e) and (f) show the corresponding normalized probability amplitude  $\tilde{R} = R(q_c, q_1, q_2) / \max[R(q_c, q_1, q_2)]$  and the contour lines of the dimensionless quantum potential  $\tilde{U}(q_c, q_1, q_2)$ .

These previous works have obtained an intuitive conclusion that squeezing interaction or squeeze state can optimize quantum synchronization. From the perspective of Bohm's interpretation, we will reexamine this issue in this section by adding squeezing-driven Hamiltonian to our model, that is,

$$H_s/\hbar = \sum_j i\eta_j \hat{b}^2 e^{-i\Lambda} + \text{H.c.}, \quad (27)$$

where  $\eta_j$  is the squeezing parameter and  $\Lambda$  determines the squeezing direction. In Figs. 9(a), 9(b), and 9(c), we respectively show the dynamic behavior of the oscillator coordinates, the coordinate error, and the phase correlation between oscillators. Compared with the case without squeezing ( $\eta_j = 0$ ), the squeezing-driven case has a quantitative impact on the shape and distribution of the Bohmian trajectories. In Fig. 9(d), we plot the corresponding limit cycle orbits in phase space. It can be seen that the limit cycle is extruded into an ellipse. On the other hand, the limit cycles at different positions are stretched to different degrees, resulting in those Bohmian trajectories no longer being parallel to each other. However, these effects are not enough to change the qualitative properties of quantum synchronization. As shown in Fig. 9(e), the quantum potential induced by squeezing-driven Hamiltonian still corresponds to a repulsive potential, so that the synchronization exhibits properties similar to the case without squeezing.

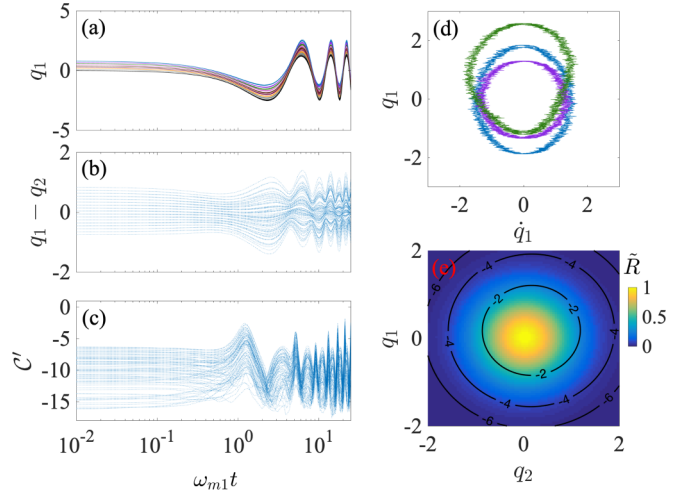


FIG. 9. Characterization of quantum synchronization with squeezing-driven Hamiltonian by using Bohmian trajectories. (a) The Bohmian trajectories corresponding to the resonators 1. (b) 81 trajectories of coordinate differences  $q_1^i - q_2^j$  obtained by Bohmian trajectories. (c) Logarithmic Pearson's correlation coefficients  $C'$  correspond to the Bohmian trajectories. (d) Orbit of Bohmian trajectory with respect of resonators 1 in the phase space span  $\{q_1, \dot{q}_1\}$ . Here the blue (bottom) limit cycle corresponds to  $q_1(0) = \sqrt{2}\langle\psi_{t_0}|\hat{b}_1|\psi_{t_0}\rangle$ ,  $q_2(0) = \sqrt{2}\langle\psi_{t_0}|\hat{b}_2|\psi_{t_0}\rangle$  (trajectory No. 41), and the green (top) limit cycle corresponds to  $q_1(0) = \sqrt{2}\langle\psi_{t_0}|\hat{b}_1|\psi_{t_0}\rangle + 0.5$ ,  $q_2(0) = \sqrt{2}\langle\psi_{t_0}|\hat{b}_2|\psi_{t_0}\rangle$  (trajectory No. 1). The purple (middle) limit cycle denotes the case of  $\eta = 0$  as a comparison. (e): The z-axis represents the normalized probability amplitude  $\tilde{R} = R(q_c, q_1, q_2) / \max[R(q_c, q_1, q_2)]$  with respect to the wave function and the contour lines corresponding to the dimensionless quantum potential  $\tilde{U}(q_c, q_1, q_2)$ . Here the parameters are the same as those of Fig. 2.

## V. CONCLUSION

In summary, we have investigated the influence of quantum effects on the continuous variable synchronization between two self-sustaining resonators in the framework of Bohmian mechanics. We have reexpressed the stochastic Schrödinger equations in the Bohmian picture, so that the self-sustaining limit cycle behavior induced by nonlinear and dissipation mechanisms in an OMS can be characterized by a series of Langevin equations with quantum potential. We have shown that the corresponding Bohmian trajectories can provide visual descriptions of quantum synchronization dynamics. As examples, we have explored the roles of zero-point fluctuation, superposition and, nonlocal correlation in synchronization dynamics. We find that the zero fluctuation corresponds to negligible repulsive potential, resulting in the behavior of Bohmian trajectories similar to semiclassical stochastic Langevin trajectories but with a more dispersed distribution. In contrast, the non-Gaussian states correspond to potential energy with complex shapes and the twisted trajectories will deviate from the single-mode oscillation according to different initial positions. Especially when we consider the Schrödinger cat state composed of two different coherent states on the limit cycle, the coherent superposition will induce some trajectories swinging between the two states, which can not be observed in the case of mixed synchronization.

Finally, we discussed the influence of the squeezing Hamiltonian on quantum synchronization. Different from the case of driven synchronization, the uncorrelated squeezed-driven case does not induce obvious disturbance or enhancement on spontaneous synchronization.

The self-sustaining dynamics of continuous-variable systems have been derived in the Bohmian picture, therefore, the synchronization analysis based on Bohmian trajectories could be extended to other forms of continuous-variable systems, such as the synchronization phenomenon between two van der Pol oscillators. On the other hand, the more significant

advantage of Bohmian mechanics is that it can give an intuitive definition and analysis for discrete variable quantum synchronization. The related discussion would be an interesting subject for future investigations.

#### ACKNOWLEDGMENTS

We acknowledge the support of the European Union Horizon 2020 Programme for Research and Innovation through the Project No. 732894 (FET Proactive HOT).

- 
- [1] C. Huygens, *Oeuvres Complètes de Christiaan Huygens* (Nijhoff, The Hague, 1893), Vol. 15, p. 243.
- [2] Y. Kuramoto, *Chemical Oscillations, Waves, and Turbulence* (Springer-Verlag, Berlin, 1984).
- [3] M. H. Xu, D. A. Tieri, E. C. Fine, J. K. Thompson, and M. J. Holland, *Phys. Rev. Lett.* **113**, 154101 (2014).
- [4] V. Ameri, M. Eghbali-Arani, A. Mari, A. Farace, F. Kheirandish, V. Giovannetti, and R. Fazio, *Phys. Rev. A* **91**, 012301 (2015).
- [5] G. L. Giorgi, F. Galve, and R. Zambrini, *Phys. Rev. A* **94**, 052121 (2016).
- [6] D. Witthaut, S. Wimberger, R. Burioni, and M. Timme, *Nature Commun.* **8**, 14829 (2017).
- [7] W. Li, F. Zhang, C. Li, and H. Song, *Commun. Nonlinear Sci. Numer. Simulat.* **42**, 121 (2017).
- [8] A. Roulet and C. Bruder, *Phys. Rev. Lett.* **121**, 053601 (2018).
- [9] A. Roulet and C. Bruder, *Phys. Rev. Lett.* **121**, 063601 (2018).
- [10] G. Karpat, İ. Yalçinkaya, B. Çakmak, G. L. Giorgi, R. Zambrini, *Phys. Rev. A* **103**, 062217 (2021).
- [11] W. Li, C. Li, and H. S. Song, *Quantum Inf. Proc.* **16**, 80 x (2017).
- [12] G. Heinrich, M. Ludwig, J. Qian, B. Kubala, and F. Marquardt, *Phys. Rev. Lett.* **107**, 043603 (2011).
- [13] C. A. Holmes, C. P. Meaney, and G. J. Milburn, *Phys. Rev. E* **85**, 066203 (2012).
- [14] G. Manzano, F. Galve, G. L. Giorgi, E. Hernández-Garcá, and R. Zambrini, *Sci. Rep.* **3**, 1439 (2013).
- [15] G. L. Giorgi, F. Plastina, G. Francica, and R. Zambrini, *Phys. Rev. A* **88**, 042115 (2013).
- [16] G. L. Giorgi, F. Galve, G. Manzano, P. Colet, and R. Zambrini, *Phys. Rev. A* **85**, 052101 (2012).
- [17] T. E. Lee and H. R. Sadeghpour, *Phys. Rev. Lett.* **111**, 234101 (2013).
- [18] A. Mari, A. Farace, N. Didier, V. Giovannetti, and R. Fazio, *Phys. Rev. Lett.* **111**, 103605 (2013).
- [19] M. Ludwig and F. Marquardt, *Phys. Rev. Lett.* **111**, 073603 (2013).
- [20] T. E. Lee, C. K. Chan, and S. Wang, *Phys. Rev. E* **89**, 022913 (2014).
- [21] L. Ying, Y. C. Lai, and C. Grebogi, *Phys. Rev. A* **90**, 053810 (2014).
- [22] T. Weiss, A. Kronwald, and F. Marquardt, *New J. Phys.* **18**, 013043 (2016).
- [23] W. Li, C. Li, and H. S. Song, *Phys. Rev. E* **93**, 062221 (2016).
- [24] F. Bemani, Ali Motazedifard, R. Roknizadeh, M. H. Naderi, and D. Vitali, *Phys. Rev. A* **96**, 023805 (2017).
- [25] W. Li, C. Li, and H. S. Song, *Phys. Rev. E* **95**, 022204 (2017).
- [26] T. Weiss, S. Walter, and F. Marquardt, *Phys. Rev. A* **95**, 041802(R) (2017).
- [27] G. J. Qiao, H. X. Gao, H. D. Liu, and X. X. Yi, *Sci. Rep.* **8**, 15614 (2018).
- [28] S. Sonar, M. Hajdušek, M. Mukherjee, R. Fazio, V. Vedral, S. Vinjanampathy, and L. C. Kwek, *Phys. Rev. Lett.* **120**, 163601 (2018).
- [29] F. A. Cárdenas-López, M. Sanz, J. C. Retamal, and E. Solano, *Adv. Quantum Technol.* **2**, 1800076 (2019).
- [30] Y. Kato, N. Yamamoto, and H. Nakao, *Phys. Rev. Research* **1**, 033012 (2019).
- [31] W. Li, P. Piergentili, J. Li, S. Zippilli, R. Natali, N. Malossi, G. Di Giuseppe, and D. Vitali, *Phys. Rev. A* **101**, 013802 (2020).
- [32] G. J. Qiao, X. Y. Liu, H. D. Liu, C. F. Sun, and X. X. Yi, *Phys. Rev. A* **101**, 053813 (2020).
- [33] N. Es'haqi-Sani, G. Manzano, R. Zambrini, and R. Fazio, *Phys. Rev. Research* **2**, 023101 (2020).
- [34] N. Jaseem, M. Hajdušek, P. Solanki, L. C. Kwek, R. Fazio, and S. Vinjanampathy, *Phys. Rev. Research* **2**, 043287 (2020).
- [35] S. E. Nigg, *Phys. Rev. A* **97**, 013811 (2018).
- [36] N. Lörch, S. E. Nigg, A. Nunnenkamp, R. P. Tiwari, and C. Bruder, *Phys. Rev. Lett.* **118**, 243602 (2017).
- [37] M. Bagheri, M. Poot, L. Fan, F. Marquardt, and H. X. Tang, *Phys. Rev. Lett.* **111**, 213902 (2013).
- [38] M. Zhang, S. Shah, J. Cardenas, and M. Lipson, *Phys. Rev. Lett.* **115**, 163902 (2015).
- [39] P. Piergentili, W. Li, R. Natali, N. Malossi, D. Vitali, and G. Di Giuseppe, *New J. Phys.* **23**, 073013 (2021).
- [40] J. Jin, D. Rossini, R. Fazio, M. Leib, and M. J. Hartmann, *Phys. Rev. Lett.* **110**, 163605 (2013).
- [41] A. Pizzi, F. Dolcini, and K. Le Hur, *Phys. Rev. B* **99**, 094301 (2019).
- [42] P. Richerme, *Physics* **10**, 5 (2017).
- [43] S. H. Choi and S. Y. Ha, *J. Phys. A: Math. Theor.* **47**, 355104 (2014).
- [44] C. Navarrete-Benlloch, E. Roldán, and G. J. de Valcárcel, *Phys. Rev. Lett.* **100**, 203601 (2008).
- [45] C. Navarrete-Benlloch, T. Weiss, S. Walter, and G. J. de Valcárcel, *Phys. Rev. Lett.* **119**, 133601 (2017).
- [46] W. Li, W. Zhang, C. Li, and H. Song, *Phys. Rev. E* **96**, 012211 (2017).
- [47] H. Halvorson and R. Clifton, *J. Math. Phys.* **41**, 1711 (2000).

- [48] M. A. Nielsen and I. L. Chuang, *Quantum Computation and Quantum Information* (Cambridge University Press, Cambridge, 2000).
- [49] H. Ollivier and W. H. Zurek, *Phys. Rev. Lett.* **88**, 017901 (2001).
- [50] D. Braun, G. Adesso, F. Benatti, R. Floreanini, U. Marzolino, M. W. Mitchell, and S. Pirandola, *Rev. Mod. Phys.* **90**, 035006 (2018).
- [51] C. Weedbrook, and S. Pirandola, and R. García-Patrón, and N. J. Cerf, and T. C. Ralph, and J. H. Shapiro, and S. Lloyd, *Rev. Mod. Phys.* **84**, 621 (2012).
- [52] H. J. Carmichael, *Statistical Methods in Quantum Optics I* (Springer-Verlag, Berlin, 1999).
- [53] H. P. Yuen and J. H. Shapiro, *IEEE Trans. Inf. Theory* **26**, 78 (1980).
- [54] A. Pikovsky, M. Rosenblum, and J. Kurths, *Synchronization: A Universal Concept in Nonlinear Sciences* (Cambridge University Press, Cambridge, 2001), Ch. 1: “Synchronization is a complex dynamical process, not a state.”
- [55] F. Marquardt, J. G. E. Harris, and S. M. Girvin, *Phys. Rev. Lett.* **96**, 103901 (2006).
- [56] D. Bohm, *Phys. Rev.* **85**, 166 (1952); **85**, 180 (1952).
- [57] X. Oriols and J. Mompar, *Applied Bohmian Mechanics From Nanoscale Systems to Cosmology* (CRC Press, Boca Raton, 2012).
- [58] S. Goldstein, *Phys. Rev. E* **60**, 7578 (1999).
- [59] Y. Song, F. M. Guo, S. Y. Li, J. G. Chen, S. L. Zeng, and Y. J. Yang, *Phys. Rev. A* **86**, 033424 (2012).
- [60] S. Dey and A. Fring, *Phys. Rev. A* **88**, 022116 (2013).
- [61] A. Budiyo and D. Rohrlich, *Nature Commun.* **8**, 1306 (2017).
- [62] C. L. Loppreore and R. E. Wyatt, *Phys. Rev. Lett.* **82**, 5190 (1999).
- [63] T. Durt and Y. Porseaux, *Phys. Rev. A* **66**, 052109 (2002).
- [64] B. Braverman and C. Simon, *Phys. Rev. Lett.* **110**, 060406 (2013).
- [65] C. R. Leavens, *Phys. Rev. A* **58**, 840 (1998).
- [66] S. Das, M. Nöth, and D. Dürr, *Phys. Rev. A* **99**, 052124 (2019).
- [67] M. Aspelmeyer, T. J. Kippenberg, and F. Marquardt, *Rev. Mod. Phys.* **86**, 1391 (2014).
- [68] D. G. Lai, J. F. Huang, X. L. Yin, B. P. Hou, W. Li, D. Vitali, F. Nori, and J. Q. Liao, *Phys. Rev. A* **102**, 011502(R) (2020).
- [69] J. P. Mathew, J. D. Pino, and E. Verhagen, *Nature Nanotechnol.* **15**, 198 (2020).
- [70] K. Fang, Z. Yu, and S. Fan, *Nature Photon.* **6**, 782 (2012).
- [71] M. Tsang and C. M. Caves, *Phys. Rev. X* **2**, 031016 (2012).
- [72] C. B. Møller, R. A. Thomas, G. Vasilakis, E. Zeuthen, Y. Tsaturyan, M. Balabas, K. Jensen, A. Schliesser, K. Hammerer, and E. S. Polzik, *Nature (London)* **547**, 191 (2017).
- [73] V. Giovannetti and D. Vitali, *Phys. Rev. A* **63**, 023812 (2001).
- [74] J. Cheng, W. Z. Zhang, L. Zhou, and W. Zhang, *Sci. Rep.* **6**, 23678 (2016).
- [75] C. W. Gardiner and P. Zoller, *Quantum Noise* (Springer, Berlin, 2000).
- [76] U. Kemiktarak, M. Durand, M. Metcalfe, and J. Lawall, *Phys. Rev. Lett.* **113**, 030802 (2014).